Universal tight binding model for chemical reactions in solution and at surfaces. III. Stoichiometric and reduced surfaces of titania and the adsorption of water

A. Y. Lozovoi,[1] D. L. Pashov,[2] T. J. Sheppard,[1] J. J. Kohanoff,[1] and A. T. Paxton[2,a)]

[1]*Atomistic Simulation Centre, School of Mathematics and Physics, Queen's University Belfast, Belfast BT7 1NN, Northern Ireland, United Kingdom*
[2]*Department of Physics, King's College London, Strand, London WC2R 2LS, United Kingdom*

We demonstrate a model for stoichiometric and reduced titanium dioxide intended for use in molecular dynamics and other atomistic simulations and based in the polarizable ion tight binding theory. This extends the model introduced in two previous papers from molecular and liquid applications into the solid state, thus completing the task of providing a comprehensive and unified scheme for studying chemical reactions, particularly aimed at problems in catalysis and electrochemistry. As before, experimental results are given priority over theoretical ones in selecting targets for model fitting, for which we used crystal parameters and band gaps of titania bulk polymorphs, rutile and anatase. The model is applied to six low index titania surfaces, with and without oxygen vacancies and adsorbed water molecules, both in dissociated and non-dissociated states. Finally, we present the results of molecular dynamics simulation of an anatase cluster with a number of adsorbed water molecules and discuss the role of edge and corner atoms of the cluster. © *2014 AIP Publishing LLC*. [http://dx.doi.org/10.1063/1.4890492]

I. INTRODUCTION

This is the last of a series of three papers presenting a universal tight binding (TB) model for the electronic structure and interatomic forces in condensed phases. The first two papers, to which we refer below as Paper I[1] and Paper II,[2] describe the application of the model to organic molecules and to polar solvents such as water. In the present paper, we extend our model to a transition metal oxide, in particular TiO_2 and analyze its bulk and surface properties, as well as its interaction with water.

Titanium oxide TiO_2 (titania) is perhaps one of the most commonly cited materials in the literature. It remains in the center of research interest for many reasons. First of all, TiO_2 is a technologically important material. Its applications include dye pigments, surface coatings, electronic devices, surgical implants, and gas sensors. TiO_2 is a promising material for photochemical reactions and for heterogeneous catalysis if used together with metal nanoparticles.

Equally important is the role of titania as a model system for studying metal oxides. Crystals of TiO_2 have relatively simple structure (rutile, anatase), are easy to prepare, stable, and have only a small amount of bulk or surface defects. Despite this, or maybe because of this, there is still a lot of controversy surrounding titania itself and its interaction with water. An in depth comprehensive review of the current state of research on titania and titania surfaces can be found in Ref. 3, whereas Refs. 4–6 provide an account of most recent progress in understanding the titania–water interaction.

The structure of the paper is as follows. Parameters of the polarizable ion tight binding (PITB) model, extended from the previous work[1,2] are listed in Sec. II and details of additional fitting procedures are given in Sec. III. Technical details about the calculations to be presented are described in Sec. IV. In Secs. V–IX we present results of simulations using the new model: In Sec. V we describe calculations in bulk, perfect TiO_2; Sec. VI contains results of simulations at semi infinite crystal surfaces, both stoichiometric (Sec. VI A) and reduced (Sec. VI B); Sec. VII contains results of simulations of water molecules, both whole and dissociated, absorbed on stoichiometric (Sec. VII A) and reduced (Sec. VII B) TiO_2 surfaces. We turn to nanocrystalline anatase particles in Sec. VIII both clean (Sec. VIII A) and decorated with absorbed water molecules (Sec. VIII B). We conclude with Sec. IX.

II. TIGHT BINDING MODEL OF TITANIA

As in Papers I and II,[1,2] we use the self consistent PITB theory described in Refs. 8–11. A concise summary can be found in Paper I.[1]

The set of model parameters sufficient to describe titania and water is presented in Table I. O–O parameters are identical to those in the TB models for water and organic molecules.[1,2]

As seen from Table I, titanium in our orthogonal non spin polarized TB model has only $3d$ states with $4s$ states completely neglected. This is possible because Ti-$4s$ states in TiO_2 are shifted into the conduction band by overlap with the oxygen $2s$ and are hence unoccupied. On the other hand, in terms of polarizability we have to go up to the quadrupole level to

a)Author to whom correspondence should be addressed. Electronic mail: Tony.Paxton@KCL.ac.uk.

TABLE I. Parameters of the TB model for titania–water system. See Ref. 1 for the meaning of parameters and abbreviations. O and H parameters are the same as in Refs. 1 and 2. Notation for the functional form of the scaling law for bond integrals and pair potential is clarified in Table II. All values are given in atomic Rydberg units.

On-site parameters				
Ti		**O**		**H**
ε_d −0.2282		ε_s −2.1164		ε_s −1
		ε_p −1.1492		
U 0.9370		U 1.0775		U 1
Δ_{ddd} 8.0		Δ_{spp} −0.9430		
Δ_{ddg} 28.0		Δ_{ppd} 0		

Bond integrals, $V_{\ell\ell'm}$, and scaling							
Ti–Ti		**Ti–O**		**O–H**		**O–O**	
Function	GSP	Function	GSP	Function	GSP	Function	GSP
$V_{dd\sigma}^0$	−0.070	$V_{ds\sigma}^0$	−0.15	$V_{ss\sigma}^0$	−0.5018	$V_{ss\sigma}^0$	−0.015
$V_{dd\pi}^0$	0.055	$V_{dp\sigma}^0$	0.18			$V_{sp\sigma}^0$	0.002
$V_{dd\delta}^0$	0	$V_{dp\pi}^0$	−0.12	$V_{ps\sigma}^0$	−0.4362	$V_{ps\sigma}^0$	−0.002
						$V_{pp\sigma}^0$	0.050
						$V_{pp\pi}^0$	−0.020
$n_{dd\sigma}$	5	$n_{ds\sigma}$	4	$n_{ss\sigma}$	2.0963	$n_{ss\sigma}$	2
$n_{dd\pi}$	5	$n_{dp\sigma}$	2.1			$n_{sp\sigma}$	2
		$n_{dp\pi}$	3.356	$n_{ps\sigma}$	1.5019	$n_{ps\sigma}$	2
						$n_{pp\sigma}$	3
						$n_{pp\pi}$	3
n_c	8	n_c	8	n_c	4.0561	n_c	6
r_0	5.55	r_0	3.685	r_0	1.8094	r_0	5.6
r_c	6.93	r_c	7.37	r_c	3.7985	r_c	9.0

Pair potentials, ϕ, and scaling							
Ti–Ti		**Ti–O**		**O–H**		**O–O**	
Function	EPL	Function	EPL	Function	GSP	Function	EPL
ϕ_1^0	0.015	ϕ_1^0	7.340×10^{-3}	ϕ^0	0.73669	ϕ_1^0	4.0306×10^{-3}
m_1	8	m_1	12	n	3.3502	m_1	10
p_1	2	p_1	0	n_c	6.3096	p_1	0
		ϕ_2^0	0.2212	r_c	3.3550	ϕ_2^0	-2.0265×10^{-3}
		m_2	1			m_2	6
		p_2	1.5933			p_2	0
r_0	5.6	r_0	3.685	r_0	1.8094	r_0	5.6

Cut-off distances $[r_{\text{cut}}^{(1)}; r_{\text{cut}}^{(2)}]$							
Ti–Ti		**Ti–O**		**O–H**		**O–O**	
$r_{\text{cut}}^{(1)}$	7.5	$r_{\text{cut}}^{(1)}$	4	$r_{\text{cut}}^{(1)}$	2.1	$r_{\text{cut}}^{(1)}$	8
$r_{\text{cut}}^{(2)}$	10.5	$r_{\text{cut}}^{(2)}$	6	$r_{\text{cut}}^{(2)}$	5.5	$r_{\text{cut}}^{(2)}$	11

describe the crystal field splitting of Ti-3d states into e_g (d_{z^2} and $d_{x^2-y^2}$ orbitals) and t_{2g} manifolds (d_{xy}, d_{xz}, and d_{yz} orbitals). This splitting is a well known feature of transition metal oxides and arises due to the octahedral coordination of Ti atoms.[3,12] Thus, our titania TB model is a quadrupole model with respect to titanium, and a dipole model with respect to oxygen.

For the scaling law of Ti–Ti and Ti–O bond integrals we use the Goodwin–Skinner–Pettifor (GSP)[1,7] dependence, whereas the Ti–Ti and Ti–O pair potentials are described as a sum of exponentials times power law (EPL) functions. Both functional dependencies, GSP and EPL, are explicitly specified in Table II.

The distance dependence of bond integrals and pair potentials is smoothly turned to zero between cutoff radii $r_{\text{cut}}^{(1)}$

and $r_{\text{cut}}^{(2)}$ using multiplicative fifth order polynomials.[2] This is necessary in order to ensure that no energy leakage or other sources of instability appear in long molecular dynamics (MD) runs. We chose to truncate Ti–O interactions between first and second neighbors in the TiO$_2$ bulk phases, resulting in relatively short Ti–O cutoff radii. Restricting interactions in solids to nearest neighbors usually leads to more reliable and physically motivated models.[13] Ti–Ti interactions, on the other hand, are more extended since there are first neighbor Ti–Ti pairs only in the rutile phase of TiO$_2$.

Titania parameters in Table I are expected to be valid not only for simulations of pure titania, but also for titania–water systems. That was the primary reason for keeping the same oxygen species in water and TiO$_2$. To make the model

TABLE II. Explicit form of the scaling laws referred to in Table I. Prefactor A denotes $V_{\ell\ell'm}^0$ in case of bond integrals and ϕ^0 in case of pair potentials.

Notation	Function	Explicit form
GSP	Goodwin–Skinner–Pettifor[7]	$f(r) = A\,(r_0/r)^n \exp\{n[-(r/r_c)^{n_c} + (r_0/r_c)^{n_c}]\}$
EPL	Exponential × Power law	$f(r) = \sum_i A_i\,(r_0/r)^{m_i} \exp[-p_i(r - r_0)]$

suitable for titania–water simulations, one needs to supply the missing Ti–H interactions. However, since Ti and H, both being positively charged ions, are not expected to approach each other, we simply neglect these interactions. Thus, Ti–H bond integrals are all set to zero, whereas the Ti–H pair potential is weakly repulsive to prevent accidental collisions between Ti and H species. A similar idea is used in Paper II[2] to specify the H–H interactions.

III. FITTING

The main challenge in the development of the titania model has been the requirement that oxygen in TiO$_2$, water, and organic molecules should be the same species. This is indeed a challenge since 2s electrons of oxygen are of primary

importance in water (in particular, their hybridization with O-2p states defines the $\widehat{HOH}$ angle in the water monomer[14]), whereas their role in titania is more modest. The TiO$_2$ valence band (in both rutile and anatase phases) is defined by the O-2p states, from which O-2s bands are separated with a wide energy gap (see Fig. 1).

As a consequence of this, titanium oxide tight binding models often ignore O-2s states altogether[13] or replace them with O-3s states.[15] The latter was the case in the TB model developed by Johnston, Benedek, and Paxton[16] in the course of their work on SrTiO$_3$ from which our TiO$_2$ fitting began.

Fitting of the model parameters started with O–O bond integrals. If these were not good enough then nothing could be corrected with other interactions such as Ti–O or Ti–Ti. At this step the nearest neighbor bond integrals were fitted to the
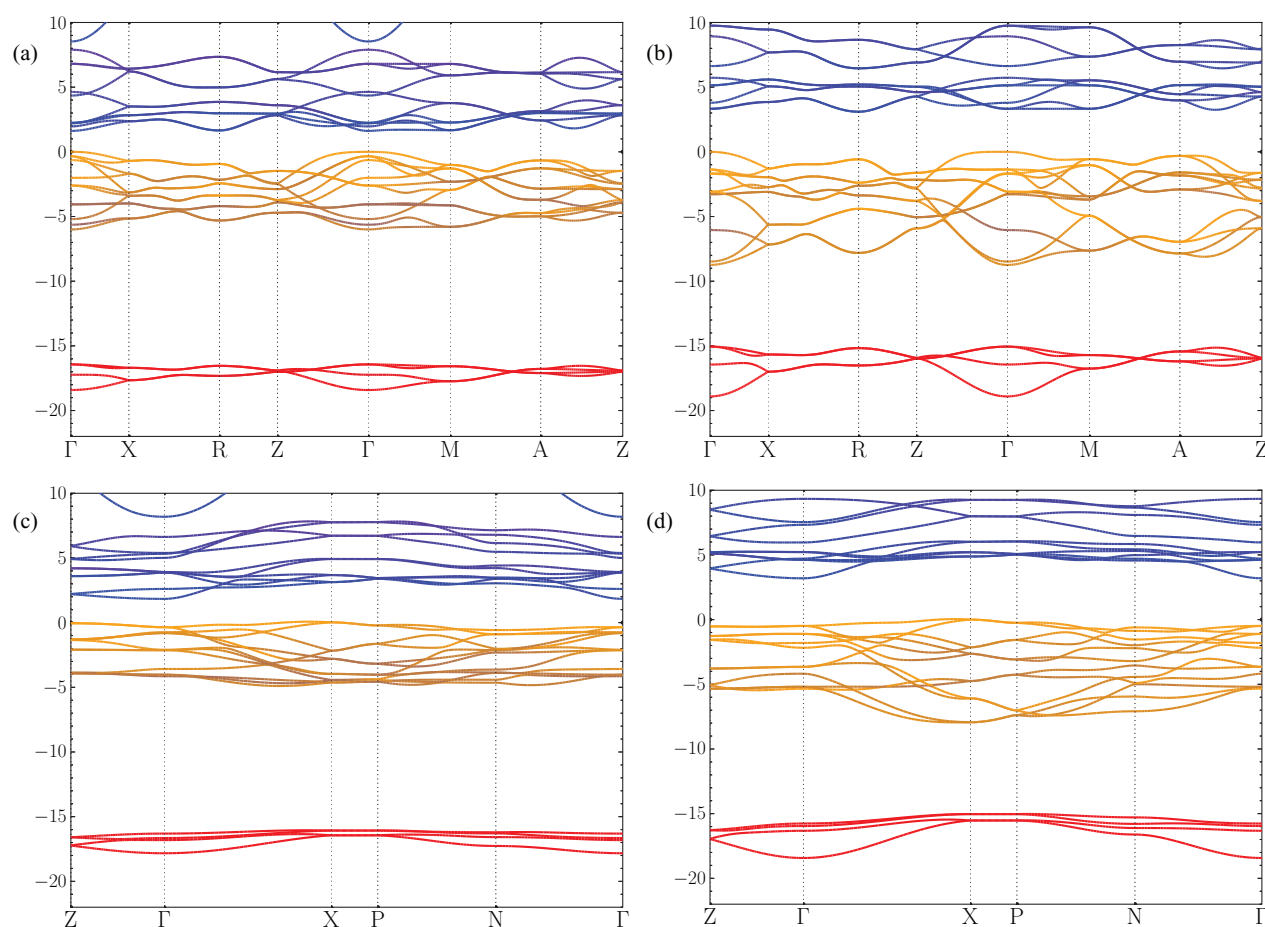

FIG. 1. Energy bands of titania polymorphs obtained at DFT and TB levels: (a) rutile, GGA (PBE); (b) rutile, TB; (c) anatase, GGA (PBE); and (d) anatase, TB. All bands are given at experimental geometry. Oxygen 2s states are shown with red color, oxygen 2p states with orange color, and other states (predominantly Ti-3d states) with blue color. Note that band gaps in TB calculations were fitted to experiment (see Table III) rather than to DFT results.

band structure of rutile and anatase at experimental geometry. The distance dependence of bond integrals (scaling laws) was not involved but rather left for subsequent steps.

Note that the above step *preceded the fitting of water*.[2] In this regard, the enumeration of papers that constitute the present three paper series is not exactly chronological: the initial O–O bond integrals were found in the present study (Paper III) and then passed to the part dealing with water (Paper II).[2] In the latter, all O–O parameters were finally established and passed to the part dealing with organic molecules (Paper I)[1] in which they were treated as fixed parameters.

In practical terms, to avoid O–O bond integrals being "damaged" at the stage of fitting the water, we estimated acceptable bounds within which the integrals can vary without causing any significant deterioration of TiO$_2$ bands. These bounds were then passed into the water fitting procedure as constraints.

As soon as the water part was finished, the whole set of O–O parameters was fixed and fitting of the rest of the titania TB model was resumed. As target quantities we used only *bulk* properties of rutile and anatase, namely, equilibrium volume, *c/a* ratio, bulk moduli, internal structural parameter, *u*, and the band gaps. These were all taken from experiment. The above properties were complemented with the equilibrium volume of fluorite and rutile–fluorite structural energy difference. Fluorite is a hypothetical phase in TiO$_2$ hence density functional theory (DFT) results were used as targets. They were assigned low weights in the objective function since the only purpose of the inclusion of fluorite was to ensure that it is much higher in energy than rutile and anatase. It is worthwhile recollecting that zirconia, on the other hand, adopts the fluorite structure, the rutile phase being much higher in energy; in fact the present PITB theory was first developed to provide insight into the structure of zirconia and the nature of its phase transitions.[8,9,15,17]

The minimization of the resulting objective function was conducted using Schwefel's genetic algorithm.[18,19] As both rutile and anatase phases are tetragonal, the full geometry optimization must include finding equilibrium volume *V* and *c/a* ratio. The straightforward search with randomly varying parameters supplied by the genetic algorithm turned out to be unstable and therefore inefficient. To circumvent the problem, in the genetic optimization we estimated the equilibrium volume and *c/a* ratio from single cross sections: *V* was obtained from the energy–volume curve at experimental *c/a*, and similarly, *c/a* was obtained at experimental volume.

After the genetic search was finished, we returned to proper geometry optimization in which both *V* and *c/a* were minimized simultaneously. That allowed us further to improve equilibrium lattice parameters, as well as the band gaps. This "fine tuning" step was performed manually as the procedure was too unstable for an automatic fitting.

IV. CALCULATION DETAILS

Tight binding calculations presented in Secs. V–VIII were all done self consistently within the PITB theory as implemented in the TBE program.[11,27] All TB models used in this study are orthogonal and do not include spin polariza-

tion. Geometry optimization was continued until Hellmann–Feynman forces became smaller than 10^{-4} Ry/Bohr and atomic displacements were less than 10^{-4} Bohr. Special **k**–point Monkhorst–Pack meshes[28] with density equivalent to the $4 \times 4 \times 4$ mesh in rutile or finer were employed for Brillouin zone sampling, whereas only the Γ point was used in MD simulations.

In MD simulations we employ reversible integrators with Liouville operators[29] and use a single Nosé–Hoover thermostat with relaxation time of 0.1 ps, exactly as in Papers I and II.[1,2] Only canonical (NVT) simulations were made in this study. Unless mentioned otherwise, MD simulations included 20–30 ps of equilibration run followed by at least 100 ps of production run with a time step of 0.5 fs.

In addition to TB studies, a few DFT calculations, using both local density approximation (LDA) and generalized gradient approximation (GGA) were done for bulk titania phases (for instance, GGA bands of rutile and anatase in Fig. 1 and LDA rutile–fluorite energy difference in Table III). For these calculations we employed the full potential LMTO program LMF which belongs to the same program suite[27] as the TBE program.

V. TITANIA BULK PHASES

Most common bulk phases of titania are rutile, anatase, and rarely, brookite. We used experimental crystal structure, bulk moduli, and band gaps of rutile and anatase to fit parameters of the TB model. Table III shows how successful we are with the fitting. As discussed in Sec. III, we also included some properties of the fluorite phase (with low weight) to ensure that fluorite is much higher in energy than rutile and anatase.

Two comments on the selection of the target values seem appropriate here. The question as to which of the two phases, rutile or anatase, is lower in energy is still a matter of debate. This is because both phases are rather stable and the energy difference is small. Experimentally rutile is considered to be the lowest energy polymorph of TiO$_2$, whereas convergent DFT GGA calculations favor anatase over rutile, and DFT LDA can predict either result.[30,31] For the fitting, we required the rutile–anatase energy difference to be as small as possible (i.e., the target was set to 0). As a result we arrived at a small negative number meaning that in our model rutile is the lowest energy structure, in apparent agreement with experiment and disagreement with DFT GGA. In Table III we include the most recent experimental result for the enthalpy of the anatase–rutile transformation that we are aware of: $\Delta H_{298} = -1.29$ mRy/f.u. (–1.70 kJ/mol).[26]

A major benefit of TB compared to DFT is that the problem of band gaps can be fixed by fitting them directly to experiment. The target band gaps shown in Table III, 3.03 eV for rutile[24] and 3.20 eV for anatase[25] are the results of seminal experiments that are frequently cited and correspond to optical band gaps. There is an ongoing discussion in the literature as to whether the fundamental band gaps would be more appropriate as targets since they do not include electron–hole interaction.[32,33] However, the current scatter of reported data is too big to make them useful as fitting targets: photoemission

TABLE III. Equilibrium crystal structure, bulk moduli, and band gaps of TiO_2 bulk phases: rutile, anatase, and fluorite. Experimental data cited were used as target values for fitting TB parameters. The exception is fluorite which is a hypothetical phase of titania, hence we used DFT results as targets instead.

	Rutile		Anatase		Fluorite	
	TB	Expt	TB	Expt	TB	DFT
			Lattice constants			
a (Å)	4.584	4.587[a]	3.771	3.782[a]	4.881[b]	4.86[c]
c (Å)	2.951	2.954[a]	9.566	9.502[a]		
V / V_{target}	0.9998	1	1.0006	1	1.0864[b]	1
Internal parameter u/a	0.303	0.305[a]	0.212	0.208[a]		
Bulk modulus (GPa)	282.1	211±7[d]	222.3	179±2[e]	330.2[f]	282[c]
Band gap (eV)	3.03	3.03[g]	3.35	3.20[h]		
			Energy differences (mRy per f.u.)			
E(rutile) – E(anatase)	–11.1	–1.29[i]				
E(fluorite) – E(rutile)[b]	67.4	51.0[j]				

[a]Neutron diffraction, Ref. 20.
[b]Used in fitting with low weight.
[c]DFT LDA, Ref. 21.
[d]X ray diffraction, Ref. 22.
[e]Reference 23.
[f]Not included into fitting.
[g]Reference 24.
[h]Reference 25.
[i]ΔH_{298}, heat capacity measurements, Ref. 26. The actual target was set to zero.
[j]DFT LDA, present study.

spectroscopy gives the electronic band gap in rutile ranging from 3.3 to 4.0 eV, which is also the range for hybrid DFT and GW predictions, whereas the situation with anatase is even worse (see, e.g., Ref. 32 and references therein). Hence, we opt to stay with the optical gaps mentioned above. This should be perfectly fine for our study dealing with only ground state simulations, as long as the band gap is wide enough to keep surface defect states confined well inside the gap.

Fig. 1 presents rutile and anatase electronic band structures obtained in DFT and our TB model. The agreement between two sets of bands is rather good, except that the underestimated DFT band gap is corrected in TB. Oxygen 2s states are well separated from oxygen 2p states which mostly constitute the valence band. The position and dispersion of states in the conduction band derived from Ti-3d electrons is also well reproduced. This is impossible to achieve within a point charge TB model.[34] It is the titanium crystal field strength parameters Δ_{ddd} and Δ_{ddg} (mostly the latter) that provide the required splitting of e_g and t_{2g} d-states by the crystal field. The fact that the direct band gap in rutile at the Γ point is nearly degenerate with the $\Gamma \rightarrow R$ indirect transition (Fig. 1(a)) is reproduced in our TB model (Fig. 1(b)) except that the $\Gamma \rightarrow R$ transition is slightly smaller than $\Gamma \rightarrow \Gamma$ (by 0.3 eV). In anatase, however, the indirect gap due to the transition from a **k**–point along the $\Gamma \rightarrow X$ direction to the Γ point (Fig. 1(c)) is rendered correctly in TB (Fig. 1(d)).

VI. TITANIA SURFACES

A. Ideal surfaces

Equilibrium surfaces of TiO_2 are studied in detail both experimentally and theoretically. The rutile (110) surface in particular is perhaps *the* model surface of a transition metal

oxide. There is a long discussion in the literature[41] of the apparent disagreement between theory and experiment in the relaxation pattern of surface atoms at rutile (110), similar to that at the α-alumina (0001) surface (see Ref. 43 and references therein) and possible reasons for the discrepancy have been suggested.[44] More careful measurements[6] and accurate DFT calculations of thicker TiO_2 slabs[41] have served partly to remove the disagreement.

For our study we selected six surfaces listed in Table IV: Rutile (110) and anatase (101) are the lowest energy surfaces, rutile (001) and anatase (001) represent high energy surfaces, whereas rutile (100) and anatase (100) are medium energy surfaces. Calculations are done with 1×1 periodic supercells containing up to 18 TiO_2 trilayers. The amount of vacuum separating periodic images along surface normal was chosen generously since in TB it does not affect the computational cost.

The even–odd oscillations that appear for some surfaces, including rutile (110),[35, 36, 38–41] are well reproduced in our calculations. This is seen in Fig. 2 where surface energy E_{surf} is plotted as a function of number of TiO_2 trilayers in the slab. The oscillations appear only after atomic relaxation takes place, and the reason for it is related to the tendency of neighboring trilayers to combine into couples thus lowering the total energy of the slab.[39] Slabs with an odd number of layers then appear at disadvantage compared to even layer slabs.

Due to the oscillations E_{surf} does not always converge even for the thickest slabs. Because of that, we list in Table IV surface energies corresponding to the two last points in Fig. 2 if the difference exceeds 0.01 J/m². Even within the remaining uncertainties, the TB surface energies are seen to fall comfortably between DFT LDA and GGA energies in
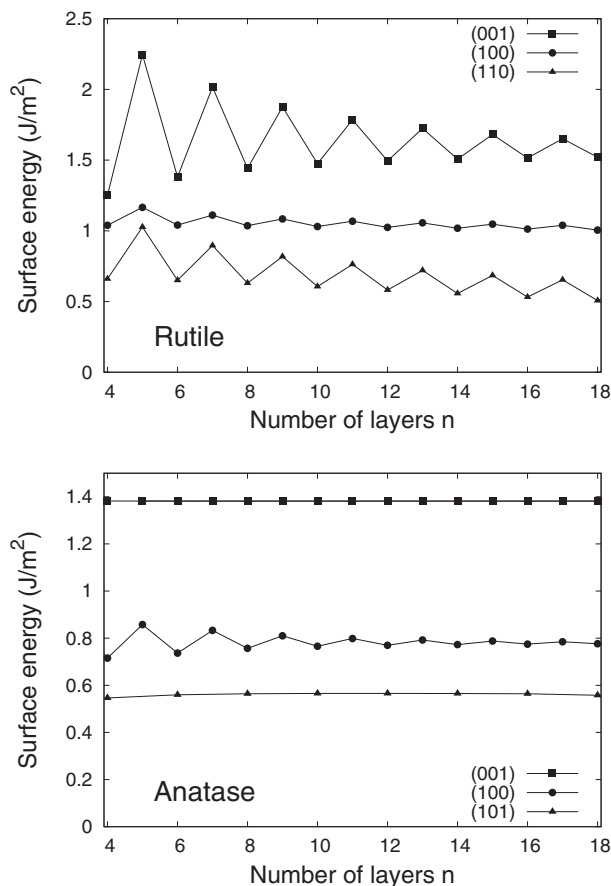
FIG. 2. Surface energy of low index surfaces of rutile (upper panel) and anatase (lower panel) as a function of slab thickness (n is the number of TiO_2 tri-layers in the slab).

Table IV. It is often assumed that LDA (GGA) tends to over-estimate (underestimate) surface energies,[45] so we are quite happy with this result especially given that none of the surface properties were included into the fitting (see Sec. III). As a matter of fact, the TB results match most closely those obtained with hybrid functionals.[35, 40, 41] In this respect, the agreement for the anatase surfaces is especially impressive. But even apart from matching particular numbers, the most important result is that the relative ordering of surface energies, namely, $E_{surf}(110) < E_{surf}(100) < E_{surf}(001)$ for rutile, and $E_{surf}(101) < E_{surf}(100) < E_{surf}(001)$ for anatase, is perfectly reproduced. That indicates that the main physics governing the cutting and resulting re-hybridization of atomic bonds in the surface region is captured in our model.

B. Reduced surfaces

Reduced titania surfaces, and in particular surfaces containing oxygen vacancies, V_O, have a significant role to play in numerous applications of TiO_2. For example, a rutile (110) unreconstructed surface annealed in UHV may contain as much as 7% of V_O residing in the surface rows of so-called bridging (doubly coordinated) oxygen atoms O_{2c}.[3] Surface vacancies are usually the most reactive sites at planar surfaces, hence their significance.

When oxygen atoms are removed from surface as neutral entities, the released electrons occupy states centered at nearby Ti atoms.[61] In a band structure picture these states fall inside the band gap and therefore are localized. Since DFT underestimates band gaps, these states can appear too close to the bottom of the conduction band, or even above it, thus becoming more delocalized than they should be. A remedy in such cases is to use LDA+U or hybrid DFT approaches.

It would therefore be a significant advantage if our TB model could handle oxygen vacancies, which is a possibility given that the bulk band gaps in both rutile and anatase are aligned with experimental ones at the fitting stage (see Sec. V). However, none of the properties related to point defects was included into the fitting; hence any encouraging results obtained for V_O would be exclusively due to the transferability of the self consistent PITB theory.

Table V lists the formation energies of an oxygen vacancy, $E^f(V_O)$, at all six titania surfaces studied in Sec. VI A. These energies are obtained by creating a single vacancy at a 3×3 cell for anatase (001) and rutile (001) and 2×4 slabs for the other surfaces, which translates into vacancy coverage of 1/9 ML and 1/8 ML, respectively. The (001) slabs contain 8 TiO_2 trilayers, rutile (110) comprises 5 TiO_2 trilayers, and the rest of the slabs contain 6 TiO_2 trilayers. Altogether, the periodic supercells include 144 atomic sites for rutile (100), 216 sites for both (001) cells, 240 sites for rutile (110), and 288 sites for anatase (101) slabs. Vacancies are placed on both sides except anatase (101) for which we use one-sided geometry.

Instead of absolute formation energies, we give in Table V energies relative to $E^f(V_O)$ at the rutile (110) surface since we do not have a reliable energy of the O_2 molecule in our non spin polarized TB model.[62] Thus, the direct comparison between TB and various DFT energies in Table V is not accessible. However, we can use results of Cheng and Selloni[46] to estimate the *difference* $E^f(V_O)$[anatase (101)]$-E^f(V_O)$[rutile (110)] for which DFT GGA (PBE) gives 0.57 eV whereas within the PBE+U approach this difference varies between 0.78 eV at $U = 3.0$ eV and 0.51 eV at $U = 4.5$ eV. The TB result is 1.54 eV and is a factor of 2–3 larger. Note, however, that because of the use of different supercells for rutile (110) and anatase (101) in DFT, the comparison we make above is approximate.

A more precise comparison between TB and DFT can be made for energy differences corresponding to exchanges of V_O between titania layers as well as for the complex TiO_2 vacancy. For the latter we again find that our TB model overestimates $E^f(V_{TiO_2})$ by a factor of two. Similar overestimation is found for the vacancy jump in rutile (110). The agreement between TB and DFT is only semi quantitative, yet we find it encouraging that in the absence of any specific effort the model already provides meaningful results. We expect that the model can be further improved to capture events at reduced titania surfaces better. It is conceivable for instance that the overestimation of vacancy formation energies is due to the omission of spin polarization effects in our model, as it leads to the reduction of degrees of freedom for the electronic subsystem.

TABLE IV. Energy of low index surfaces of rutile and anatase (in J/m^2): TB prediction in comparison with LDA, GGA, and hybrid DFT results. Due to oscillatory convergence of surface energy with slab thickness (see Fig. 2) TB surface energies are given for both 17- and 18-trilayer slabs if the difference between them exceeds 0.01 J/m^2.

Surface	TB	LDA	GGA PBE	Hybrid B3LYP	PBE0	PW1PW
			Rutile			
(110)	0.51–0.65	0.89[a]	0.42,[a] 0.31[b]	0.40[a]	0.55[a]	0.62[c]
			0.47,[d] 0.36[e]		0.57[f]	
(100)	1.01–1.04	1.20[a]	0.69[a]	0.70[a]	0.83[a]	0.85[c]
					0.85[f]	
(001)	1.52–1.65	1.88[a]	1.39[a]	1.45[a]	1.59[a]	1.47[c]
					1.55[f]	
			Anatase			
(101)	0.56	0.83[a]	0.50,[a] 0.44[b]	0.55[a]	0.60[a]	0.64[c]
(100)	0.78	0.97[a]	0.63,[a] 0.53[b]	0.67[a]	0.73[a]	0.81[c]
(001)	1.38		0.98,[g] 0.90[b]			1.36[c]

[a]Reference 35.
[b]References 36 and 37.
[c]Reference 41.
[d]Reference 38.
[e]Reference 39.
[f]Reference 40, data taken from graph.
[g]Reference 42.

TABLE V. Formation energies E^f (in eV) of oxygen vacancies and related defects at pure titania surfaces. TB formation energies of isolated oxygen vacancies are given relative to that at the rutile (110) surface. DFT vacancy formation energies are the absolute energies obtained in the oxygen–rich limit.

Surface	Site (jump type)	TB	DFT	DFT +U	Hybrid DFT
	Surface oxygen vacancy (layer 1)				
Rutile(110)	O_{2c}	0[a]	3.68[b]	2.88[b]	
			3.02[c]		
			3.85[d]		
Rutile(100)	O_{2c}	0.22[a]			
Rutile(001)	O_{2c}	1.18[a]			
Anatase(101)	O_{2c}	1.54[a]	4.25[b]	3.39[b]	
Anatase(100)	O_{2c}	1.18[a]			
Anatase(001)	O_{2c}	0.13[a]			
	Oxygen vacancy jumps				
Rutile(110)	Layers 1 → 2	1.70	0.82[b]		
			0.98[c]		
			1.14[d]		
	Layers 1 → 4		1.55[b]	0.51[b]	
Anatase(101)	Layers 1 → 2	0.21	1.15[b]		
	Layers 2 → 3	0.17	−0.67[b]		
	Layers 3 → 4	0.01	−0.70[b]		
	Layers 1 → 4	0.38	−0.22[b]	0.33[b]	−0.61[e]
	TiO$_2$ vacancy				
Rutile(110)	$Ti_{5c} + 2O_{2c}$	2.05	1.03[c]		

[a]TB V_O formation energies are given relatively to that at rutile(110) surface.
[b]PBE and PBE+U, Ref. 46. PBE+U results are cited for $U = 4.5$ eV.
[c]PBE, Ref. 39.
[d]PBE, Ref. 47.
[e]PBE0, Ref. 48.

To proceed, we now consider vacancy exchanges at anatase (101) and rutile (110) surfaces. It was discovered by Cheng and Selloni (see Ref. 46 and references therein) that DFT GGA (PBE) predicts subsurface V_O to be lower in energy than V_O at the surface layer as seen in Table V (the layer 4 vacancy site is situated directly below the layer 1 vacancy site). PBE+U results are not conclusive in this respect: the layer 4 vacancy is more stable than layer 1 vacancy at $U = 2.5$ eV but at $U = 4.5$ eV this is reversed. In a more recent study combining STM measurements and hybrid PBE0 calculations, the subsurface vacancy was again found more favorable.[48] In our TB model the preference of the subsurface site is not reproduced: the TB prediction is that the layer 1 → layer 4 jump costs 0.38 eV, which agrees with the PBE+U result of 0.33 eV (with $U = 4.5$ eV) but disagrees with plain PBE and hybrid PBE0 values of –0.22 eV[46] and –0.61 eV,[48] respectively.

For rutile (110) the first layer vacancy is the lowest energy according to both TB and DFT, although TB again overestimates the energy of the vacancy jump from the bridging oxygen row into the in-plane position in the surface layer by a factor of two. Note in passing that our TB model predicts the following ordering of surface vacancies in energy: rutile (110) < anatase (001) ≃ rutile (100) < rutile (001) ≃ anatase (100) < anatase (101). In fact it is well known that oxygen vacancies at the (110) surface of rutile are easily created by thermal annealing,[3] whereas oxygen vacancies at anatase (101) have such high energy that they migrate into the bulk of the material during annealing.[48]

It is interesting that surface vacancy formation energies do not show any correlation with surface energies. In particular, the vacancies with the highest and lowest energy from the above list are those at rutile (110) and anatase (101), which are both the lowest energy surfaces of rutile and anatase, respectively.

VII. ADSORBED WATER MOLECULES

One of the reasons for developing our TB model in the way we did, was to make it possible to simulate complex systems with both titania and water present. An isolated water molecule adsorbed on TiO$_2$ surfaces is, perhaps, the simplest type of a water–titania system. Yet it would be impossible to study the adsorption of water into an oxygen vacancy if oxygen of water and oxygen of titania were not the same species. In Sec. VII A, we look first into the water adsorption on ideal TiO$_2$, and then, in Sec. VII B, present our results for the adsorption on reduced titania.

A. Adsorption at ideal surfaces

Water readily adsorbs on TiO$_2$ as has been known since the seminal discovery of the fact that titania can split adsorbed water into O$_2$ and H$_2$ molecules by means of photolysis.[64] Nevertheless, the question as to whether a single water molecule dissociates on the (110) surface of rutile still remains under intensive debate. Most experimental studies suggest that water molecules should dissociate on all titania surfaces except perfect unreconstructed rutile (110) and anatase (101).[3,5] However, some recent experimental studies of ideal rutile (110) terraces report dissociated water molecules which are not related to oxygen vacancies, surface steps, or other types of surface defects.[65,66] An interesting explanation was proposed by Walle *et al.*[67] who suggested that water molecules already dissociated at V$_O$ could impede the dissociation for other molecules, which is why the dissociated molecules are observed in some studies and not observed in others.

Theoretical computations (mostly DFT) produce results of either type, as the water adsorption energies, both in the associated (molecular) state, E_{ads}^{mol}, and in the dissociated state, E_{ads}^{dis}, strongly depend on computational details, such as the coverage, slab width, relaxation constraints, and the exchange–correlation functional employed. This is illustrated in Table VI in which we cite a few (out of many) recent calculations corresponding to coverage $\Theta = 1/4$ and lower, and to slab thickness of at least four TiO$_2$ trilayers.

Our TB results for rutile (110) favor dissociated water in agreement with Refs. 39 and 54 and in disagreement with Refs. 53, 55, and 56. In its absolute value, E_{ads}^{mol} is in excellent agreement with DFT results and experiment, but E_{ads}^{dis} seems overestimated. In order to get a better understanding of the water dissociation process, we made a number of 50 ps long MD NVT simulations at temperatures 300 K, 400 K, 500 K, and 600 K. Since TB predicts E_{ads}^{dis} almost twice as negative as E_{ads}^{mol}, one would expect dissociation to happen straight away. However, only in one simulation did we observe water disso-

ciation at $T = 500$ K. At 300 K and 400 K we did not detect any events, at 500 K water molecules mostly diffused along the surface instead of dissociating, and at 600 K they moved along rows of bridging oxygens, jumped over them, formed hydrogen bonds with bridging oxygens, and eventually left the surface. It is possible that the observed behavior might be relevant to the reluctance of water to dissociate on the perfect (110) surface of rutile.

For the water adsorption on rutile (100) surface, TB predicts the dissociated and non-dissociated states to be close in energy, with a slight preference for the dissociation. PBE calculations by Kamisaka and Yamashita[53] favor the non-dissociated state by 0.25 eV (see Table VI), whereas experimentally both dissociative and molecular adsorption are observed—the current view is that water initially adsorbs dissociatively, followed by the molecular adsorption at higher coverage.[3]

The rutile (001) surface (see Table IV) has only fourfold coordinated Ti$_{4c}$ and twofold coordinated O$_{2c}$ exposed. As a result, it is less stable than other surfaces and tends to facet or reconstruct. Hence, it is not a common subject for experimental and theoretical investigation. A few existing studies agree on the dissociative water adsorption.[3] TB also predicts that dissociative adsorption is favored by 0.37 eV.

In the anatase part of Table VI we observe a good agreement between TB results and DFT results for all three surfaces: (101), (100), and (001). Dissociation is not favored for anatase (101), but is favored on (100) and (001) surfaces, with a sizable energetic effect in the latter case. This is the only case in which the dissociation occurs straight away in our MD simulations, and it takes only 3–6 ps to happen. A large negative E_{ads}^{dis} for the anatase (001) surface is also found in DFT GGA calculations.[42,60]

Overall we conclude that our TB model adequately describes the principal features related to water adsorption and dissociation at ideal stoichiometric titania surfaces.

B. Adsorption at reduced surfaces

Experiment suggests that the adsorption of a water molecule into an oxygen vacancy at the (110) surface of rutile should lead to straight decomposition of H$_2$O into two hydroxyl groups situated next to each other in the bridging oxygen row.[5] PBE[53,57] and PBE+U[57] simulations confirm that the dissociated molecule has a large negative adsorption energy, especially within the PBE+U approach (see the "(110) + V$_O$" row in Table VI). The TB prediction is that both E_{ads}^{mol} and E_{ads}^{dis} are large and negative, with E_{ads}^{dis} being lower. That means that the adsorbed H$_2$O molecule should dissociate, in apparent agreement with experiment.

A closer inspection of the TB data, however, reveals that it is more favorable for an adsorbed molecule on the reduced surface to move onto a nearest neighbor (NN) Ti$_{5c}$ site and then further down to the next nearest neighbor (NNN) or third nearest neighbor (3NN) Ti$_{5c}$ site and to dissociate there. In fact, that was exactly the behavior we observed in an MD NVT simulation of H$_2$O adsorbed into an oxygen vacancy on rutile (110), at least in the initial stages of the simulation: the

TABLE VI. Adsorption energies (in eV) of a water molecule in the dissociated E_{ads}^{dis} and molecular state E_{ads}^{mol}, together with the dissociation energy $\Delta E_{diss} = E_{ads}^{dis} - E_{ads}^{mol}$. Adsorption sites NN, NNN, and 3NN refer to the nearest neighbor, next nearest neighbor, and third nearest neighbor Ti site as seen from the oxygen vacancy on reduced titania surfaces. The sign convention is that a negative adsorption/dissociation energy favors adsorption/dissociation. For an extended compilation of recent DFT results see Refs. 4 and 49.

Surface	Adsorption site	TB			DFT (GGA)			GGA+U			Experiment
		E_{ads}^{mol}	E_{ads}^{diss}	ΔE_{diss}	E_{ads}^{mol}	E_{ads}^{diss}	ΔE_{diss}	E_{ads}^{mol}	E_{ads}^{diss}	ΔE_{diss}	
					Rutile						
(110)	Ti$_{5c}$	−0.92	−1.72	−0.79	−0.93[a]	−1.04[a]	−0.11[a]				−0.73,[b] −0.72,[b] −0.79[b]
					−0.70[c]	−0.46[c]	0.24[c]				
					−0.49[d]	−0.68[d]	−0.19[d]				
					−0.76[e]	−0.66[e]	0.10[e]				
					−0.95[f]	−0.90[f]	0.05[f]				
(110)+V$_O$	O$_{2c}$	−1.43	−2.06	−0.63		−1.30[c]					
						−1.18[g]			−1.61[g]		
	NN Ti$_{5c}$	−1.44	−1.68	−0.24	−0.80[g]	−0.89[g]	−0.09[g]	−0.77[g]	−0.87[g]	−0.10[g]	
	NNN Ti$_{5c}$	−1.57	−2.18	−0.61	−0.81[g]	−0.95[g]	−0.14[g]	−0.83[g]	−0.92[g]	−0.09[g]	
	3NN Ti$_{5c}$	−1.56	−1.92	−0.36	−0.82[g]	−0.90[g]	−0.08[g]	−0.84[g]	−0.89[g]	−0.05[g]	
(100)	Ti$_{5c}$	−1.07	−1.10	−0.03	−0.91[c]	−0.66[c]	0.25[c]				
(100)+V$_O$	O$_{2c}$	0.31	−0.52	−0.83		−1.39[c]					
	NN Ti$_{5c}$	−0.43	−0.37	0.06							
	NNN Ti$_{5c}$	0.35	0.27	−0.08							
(001)	Ti$_{4c}$	−1.14	−1.51	−0.37							
(001)+V$_O$	O$_{2c}$	−1.01	−2.41	−1.18							
	NN Ti$_{4c}$	−0.42	−0.32	0.10							
	NNN Ti$_{4c}$	−0.37	−0.09	0.28							
					Anatase						
(101)	Ti$_{5c}$	−0.81	−0.52	0.29	−0.73[h]						−0.69[i]
					−0.95[j]	−0.66[j]	0.29[j]				
(101)+V$_O$	O$_{2c}$	−1.22	−2.45	−1.23							
	NN Ti$_{5c}$	−0.75	−0.55	0.20							
	NNN Ti$_{5c}$	−0.57	−0.43	0.14							
(100)	Ti$_{5c}$	−0.70	−1.15	−0.46	−0.74[j]	−0.78[j]	−0.03[j]				
(100)+V$_O$	O$_{2c}$	−1.11	−2.22	−1.11							
	NN Ti$_{5c}$	−1.11	−2.24	−1.14							
	NNN Ti$_{5c}$	−0.51	−1.25	−0.74							
(001)	Ti$_{5c}$	−0.58	−2.33	−1.76	−1.15[j]	−2.84[j]	−1.68[j]				
						−1.25[k]					
(001)+V$_O$	O$_{2c}$	−1.05	−3.06	−2.01							
	NN Ti$_{5c}$	−0.34	−2.47	−2.13							
	NNN Ti$_{5c}$	−0.64	−2.46	−0.64							

[a]Reference 39: PBE, $\Theta = 1/8$, 4 layer TiO$_2$ slab, one–sided adsorption with passivation.
[b]Temperature-programmed desorption: adsorption energies as a function of coverage $(71 − 9\Theta)$ kJ/mol [Ref. 50], $(70 − 7\Theta)$ kJ/mol [Refs. 51 and 52], and $(80 − 35\Theta)$ kJ/mol [Ref. 52], respectively, interpolated into $\Theta = 1/8$ and converted into eV units.
[c]Ref. 53: PBE, $\Theta = 1/3$ for (110) surface and $\Theta = 1/4$ for (100) surface, 4 layer TiO$_2$ slab, one–sided adsorption.
[d]Reference 54: RPBE, $\Theta = 1/4$, 5 layer TiO$_2$ slab, two–sided adsorption.
[e]Reference 55: PBE, $\Theta = 1/4$, 4 layer TiO$_2$ slab, one–sided adsorption.
[f]Reference 56: PW91, $\Theta = 1/5$, 5 layer TiO$_2$ slab, two–sided adsorption.
[g]Reference 57: PBE and PBE+U with $U = 4.2$ eV, $\Theta = 1/8$, 4 layer TiO$_2$ slab, one–sided adsorption with passivation.
[h]Reference 58: PBE, $\Theta = 1/4$, 4 layer TiO$_2$ slab.
[i]Reference 59: Temperature-programmed desorption.
[j]Reference 60: PBE, $\Theta = 1/9 − 1/4$ depending on surface, 8 layer TiO$_2$ slab with 4 bottom layers fixed, one–sided adsorption.
[k]Reference 42: PBE, $\Theta = 1/6$, 4 layer TiO$_2$ slab, one–sided adsorption.

molecule eventually vacates the V$_O$ site and moves along the [001] direction to the NNN Ti$_{5c}$ site. We never managed to observe dissociation in our relatively short runs for reasons discussed in Sec. VII A. This scenario, however, is not supported by DFT results,[57] according to which H$_2$O dissociation at V$_O$ corresponds to the lowest energy, both in PBE and PBE+U. Note in passing that TB adsorption energies appear a factor of two larger than their DFT counterparts.

Rutile (100) is another surface for which there are DFT data with which to compare. Kamisaka and Yamashita[53] report E_{ads}^{dis} for water in the vacancy to be lower than E_{ads}^{mol} at the regular Ti$_{5c}$ site on the ideal surface, which is in turn lower than E_{ads}^{dis} on the ideal surface: E_{ads}^{dis}(reduced) $< E_{ads}^{mol}$(ideal) $< E_{ads}^{dis}$(ideal). Our TB prediction is exactly the opposite: E_{ads}^{dis}(reduced) $> E_{ads}^{mol}$(ideal) $> E_{ads}^{dis}$(ideal). As a matter of fact, TB results for the rutile (100) surface stand out from
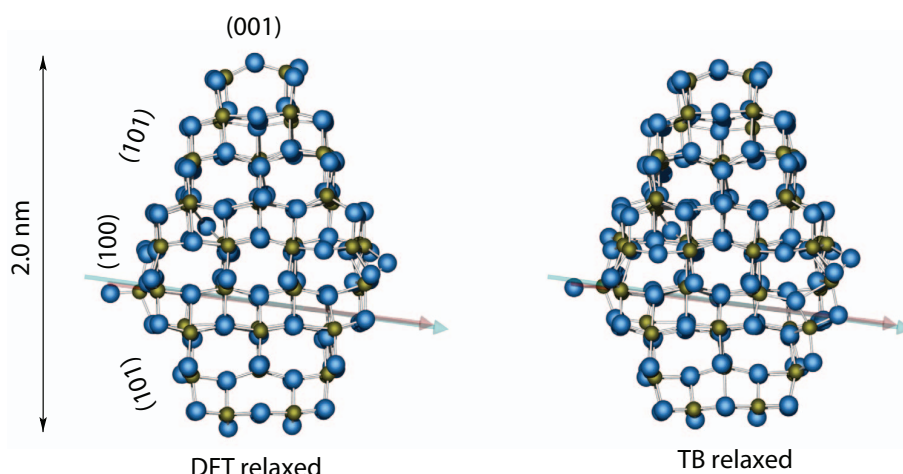
FIG. 3. Equilibrium geometry of a 234 atom anatase cluster obtained with DFT GGA (PBE)[63] (left panel) and with TB (right panel). Titanium and oxygen atoms are shown with green and blue spheres, respectively. Arrows (same on both panels) show the direction and relative magnitude of the spontaneous dipole which the clusters develop: 11.18 D in the PBE relaxed geometry (pink arrow) and 12.04 D in the TB relaxed geometry (light blue arrow).

those for other surfaces. For instance, molecular adsorption into V_O results in significant relaxation of the top layer during which the O atom of adsorbed water molecule breaks its bond with one of the neighboring Ti atoms and tries to reach out to another O atom from the opposite row to form a H-bond with it. This leads to a pronounced distortion in surrounding atoms resulting in a positive E_{ads}^{mol}. It would be interesting to investigate the reduced rutile (100) surface with water using a more accurate approach, although there is, of course, a possibility that some of the TB predictions can be just an artefact of the present model.

For all other reduced surfaces listed in Table VI, TB predicts that water dissociation at an oxygen vacancy always leads to the lowest energy. This is true even for anatase (101) for which dissociation at the ideal surface is unfavorable. This is a plausible result, although more generally it seems that the good performance of the TB model observed for water adsorption at ideal surfaces somewhat worsens for reduced titania surfaces.

VIII. ANATASE CLUSTERS

There has been a surge of interest in titania clusters lately. TiO$_2$ clusters are easy to prepare and they keep a good degree of crystallinity down to nanometer sizes. Nanosize samples are found to possess a number of attractive features, such as enhanced electrical properties and photocatalytic activity (see Refs. 68 and 69, and references therein). Expected enhancement of the surface reactivity of nanoclusters compared to macroscopic samples could be equally important. In this section we restrict ourselves to the anatase polymorph since this is the stable form of TiO$_2$ clusters smaller than 14 nm.[70]

A. Free standing clusters

We begin by considering isolated stoichiometric clusters of anatase. A typical shape of a cluster shown in Fig. 3 for a 234 atom cluster and in Fig. 4 for a 1233 atom cluster

has {101}, {100}, and {001} faces exposed. The equilibrium Wulff shape of anatase crystals according to DFT surface energies and that found in natural minerals has only {101} and {001} facets.[3] However, the equilibrium shapes of small particles can differ from the Wulff shape since the Wulff construction neglects any energy associated with edges and corners.[68] In particular, the {100} facet was indeed detected in anatase powder.[3]

The geometry of the clusters shown in Figs. 3 and 4 was optimized using DFT GGA (PBE)[63] and TB. The relaxed atomic positions significantly deviate from the initial ideal bulk positions (not shown), but in both cases the relaxation process ends up in similar geometries. This can be seen from
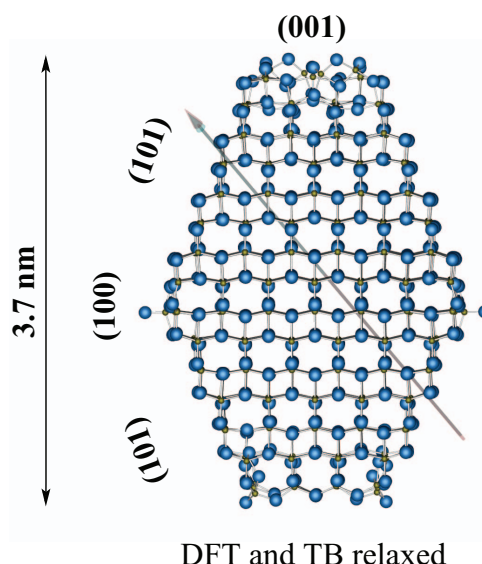

FIG. 4. Same as Fig. 3 except for a bigger cluster (1233 atoms). The difference between geometries obtained by DFT GGA (PBE)[63] and TB is indistinguishable on the figure scale, thus only one instance of the cluster is shown. Pink and light blue arrows correspond to dipoles 11.32 D (PBE–relaxed geometry) and 10.87 D (TB–relaxed geometry), respectively.

the comparison of DFT relaxed (left panel) and TB relaxed (right panel) structures of the 234 atom cluster in Fig. 3. A relaxation of the 1233 atom cluster results in geometries practically indistinguishable on the plotted scale, therefore in Fig. 4 we show only the TB relaxed cluster.

A closer inspection of the TB results reveals that during atomistic relaxation clusters develop spontaneous dipole moments losing in the process the original symmetry of the cluster. The dipole was found both in the relaxed TB geometry and in the relaxed DFT geometry as indicated in Figs. 3 and 4 with blue and pink arrows, respectively. The loss of symmetry and spontaneous polarization of the clusters is an interesting effect which might not be completely surprising given the propensity of titania to ferroelectricity. Thus, a ferroelectric phase transition at negative pressure $p \simeq -4$ GPa was predicted by Montanari and Harrison[71] on the basis of DFT analysis of phonon modes in rutile.

The magnitude of the spontaneous dipole in anatase, namely, about 10 D, is modest but not negligible—for comparison, the dipole of a water molecule in the gas phase is only 1.84 D. The formation of a spontaneous electrostatic dipole in *water* clusters with radius up to 3 nm was observed by Lever *et al.*[72] in DFT and force field simulations. It remains to be seen whether these effects are related.

B. Anatase cluster with water

We consider next the interaction of an anatase cluster and water molecules. There are a number of interesting questions one can immediately pose, such as: (i) Do the adsorption preferences of water molecules follow those at flat surfaces? (ii) Do water molecules dissociate better on clusters compared to planar semi infinite surfaces? (iii) What rôle is played by edge and corner atoms of a cluster? And ultimately, (iv) Are cluster surfaces more reactive than those of semi infinite crystals?

In order to obtain some insight into these questions we made MD simulations in a canonical ensemble at three temperatures: $T = 300$ K, 400 K, and 500 K. For our simulations we employ a 230 atom anatase cluster from Ref. 73. It has 78 TiO_2 units and four oxygen vacancies, so it is a reduced titania sample. Contrary to the similar 234 atom stoichiometric cluster shown in Fig. 3, it does not have any "loose" oxygen atoms, such as those seen in the equatorial plane in Figs. 3 and 4, which makes it more suitable for MD simulations.

We first statically relaxed the cluster with 15 water molecules randomly placed around it until forces were smaller than 10^{-4} Ry/Bohr. In the relaxed configuration, all 15 H_2O molecules absorb on the surface, forming bonds with Ti atoms. The average adsorption energy per molecule, –0.82 eV, can be compared to those at planar surfaces $E_{ads}^{mol}(101) = -0.81$ eV, $E_{ads}^{mol}(100) = -0.70$ eV, and $E_{ads}^{mol}(100) = -0.58$ eV, whereas the corresponding vacancy adsorption energies are by 0.4 eV lower (see Table VI). The HOMO–LUMO gap of the relaxed cluster, 2.0 eV, is significantly reduced compared to the band gap of bulk anatase, 3.35 eV in our model (see Table III). The static relaxation step was followed by 120–160 ps of equilibration, after which we col-

TABLE VII. Temperature T, length of production run τ, average proportion of water molecules adsorbed on facets (water/Ti_{5c}), on edges/corners of the cluster (water/Ti_{4c}), and of unattached molecules (see Fig. 6 for the trajectory profiles). The last two lines show the average number of H-bonds formed between two water molecules $\langle O_w - H \cdots O_w \rangle$ and between a water molecule and titania's O atom $\langle O_w - H \cdots O_t \rangle$ (see Fig. 7 for the respective histograms).

T [K]	300	400	500
length of MD run τ [ps]	144	134	152
$\langle n(\text{water}/Ti_{5c}) \rangle / n_w^{tot}$	45.87%	53.08%	42.61%
$\langle n(\text{water}/Ti_{4c}) \rangle / n_w^{tot}$	52.99%	45.98%	33.34%
$\langle n(\text{unattached water}) \rangle / n_w^{tot}$	0	0.02%	22.82%
$\langle O_w - H \cdots O_w \rangle$	0.17	0.068	0.0066
$\langle O_w - H \cdots O_t \rangle$	20.99	20.69	13.13

lected data during the next 130–150 ps of production run (see Table VII).

One of the snapshots, shown in Fig. 5, demonstrates a few typical features of molecular arrangement during MD simulations. A number of water molecules indeed attach to the
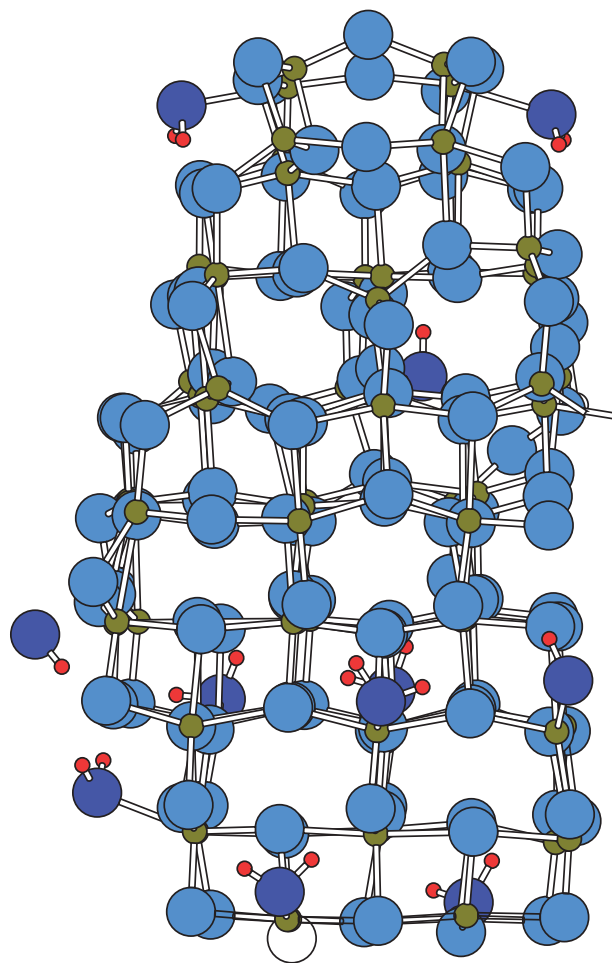

FIG. 5. A snapshot of MD simulation of the 230 atom anatase cluster with 15 water molecules at $T = 500$ K. Green spheres are Ti atoms, red spheres are H atoms, blue and light blue spheres are O atoms of water and titania, respectively. O of course is the same species in both cases, it is painted differently only for convenience.

(101) faces of the cluster which provide the lowest adsorption energy for planar surfaces, at least in our model. We also note five H_2O molecules attached to the edge of the (001) face (two at the top, and three at the bottom of the cluster in Fig. 5) that lean toward the (101) facet and form H-bonds with O atoms on it. This configuration appears to be very stable, it persists in all three MD simulations with minor modifications. There are also two water molecules on the right hand side of the cluster (in the equatorial region) that form a H-bonded chain $Ti-O_w-H\cdots O_w-H\cdots O_t$ (here and below O_w and O_t denote oxygen atoms of water and titania, respectively). This is a significantly less frequent event. And on the opposite side of the cluster, there is a water molecule moving along the surface and forming H-bonds along its way.

A surprising result coming from our simulation is the fact that *none* of the H_2O molecules dissociated in any of the MD runs. Even a molecule adsorbed on the (001) face, for which it takes only 3–6 ps to dissociate on an infinite (001) surface (see Sec. VII A), stays intact and either leans toward the (101) facet or diffuses away along the cluster. One of the reasons for high reactivity of the (001) surface of anatase towards water dissociation is a rather strained geometry of the surface layer.[42] However, it is much easier to reduce such strain for atoms in a small cluster compared to a semi infinite crystal. Perhaps, that can explain the reluctance of water molecules to dissociate. More generally, there are indications that water should dissociate more readily on anatase clusters compared to macroscopic crystals (see Ref. 74 and references therein). Our simulations do not corroborate this expectation, at least not for a nanocluster as small as 2 nm in size.

We consider next the competition between adsorption onto facets, edges, and corners of a nanocrystallite. To formally distinguish between these sites we use the O coordination number of Ti atoms evaluated in the initial bulk truncated geometry of the cluster. Bulk atoms have 6 oxygen neighbors, surface atoms have 5, whereas edge and corner atoms have 4 neighbors each. We keep this classification of Ti atoms along all three MD trajectories, assuming that $Ti-O_t$ bonds do not cleave or reform.[75]

The relative number of adsorbed water molecules taken along the trajectories is shown in Fig. 6. There are 12 Ti_{4c} atoms and 40 Ti_{5c} atoms in the cluster. However, the $T = 300$ K results show that the adsorbed molecules split almost equally between two types of sites, with the Ti_{4c} even having some advantage (53% *vs.* 46% according to Table VII). This indicates that edges and corners are more favorable than the (101), (100), and (001) facets. In the $T = 400$ K simulation, this picture changes to its opposite: now 46% water molecules occupy Ti_{4c} sites and 53% molecules adsorb on Ti_{5c}. This is a clear manifestation of the entropic contribution to the free energy since 40 Ti_{5c} sites have larger configurational entropy than 12 Ti_{4c} sites. If the trend continues, one would expect occupations to tend to 23% and 77% in the hypothetical high temperature limit. However, at $T = 500$ K both occupations decrease to 33% and 43%, respectively, because at this temperature the onset of water evaporation is observed on the simulation time scale. By the end of 150 ps of equilibration, the 500 K system has already lost three out of 15 water molecules. A fourth molecule flew away after 90 ps of the production run
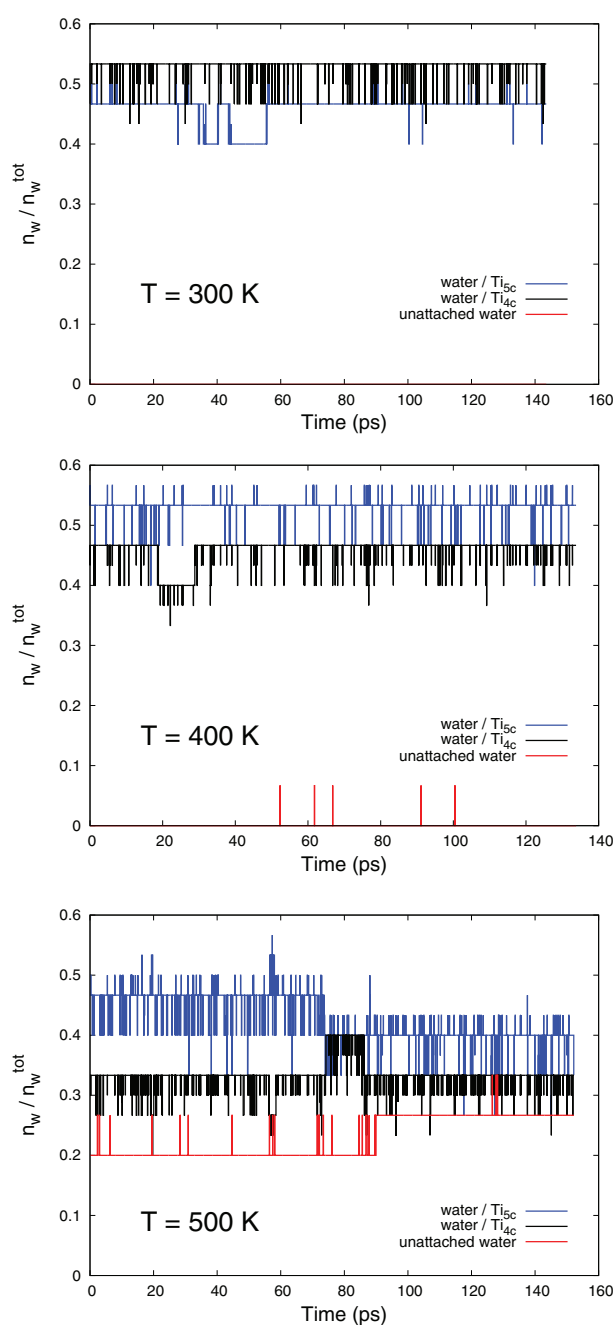

FIG. 6. Fraction of water molecules, n_w/n_w^{tot} (where $n_w^{tot} = 15$) adsorbed on 5-fold coordinated titanium atoms Ti_{5c} (blue line), 4-fold coordinated titanium atoms Ti_{4c} (black line), and of unattached molecules (red line) collected along the trajectory of three NVT simulations at 300 K (top panel), 400 K (middle panel), and 500 K (bottom panel). See Table VII for the average quantities.

(see red line in Fig. 6). Overall, in the adsorption behavior we clearly see an interplay between potential energy and entropic contribution, affected by adsorbate evaporation at higher temperatures.

Finally, we look at the formation of hydrogen bonds in the system. Do water molecules prefer to form H-bonds with the substrate or with each other? The answer is the former, as is clear from Table VII and Fig. 7. This is not because the
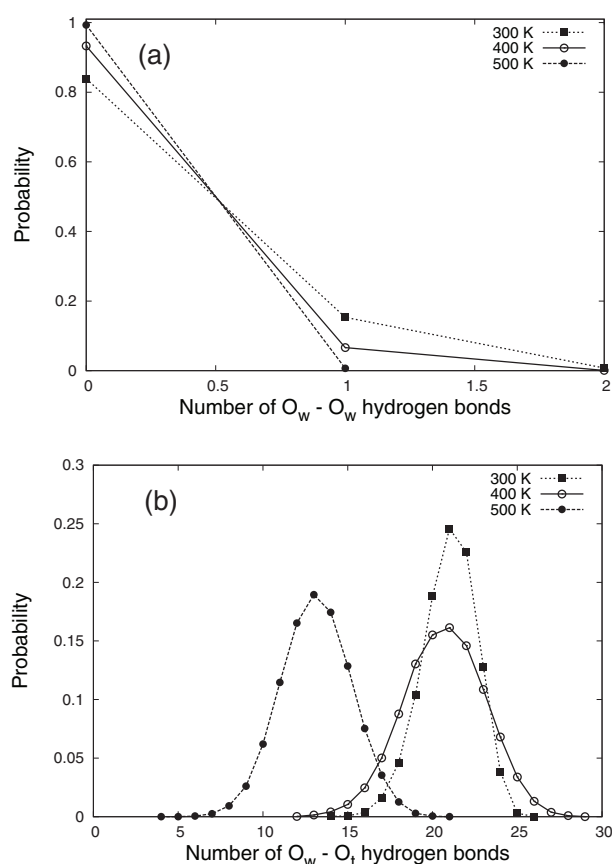
FIG. 7. Histograms showing the number of hydrogen bonds (a) between two water molecules and (b) between a water molecule and titania's oxygen atom (O_t). See Table VII for the average number of H-bonds.

O_w–H···O_t bond is much stronger than the O_w–H···O_w bond but rather because the O_w–H···O_t bonds are formed *in addition* to the adsorption onto Ti sites (see Fig. 5), so it is in fact the competition between the Ti–O_w–H···O_t and O_w–H···O_w bonds. Not surprisingly, only a small fraction of frames have at least one water–water H-bond (15% at 300 K, 7% at 400 K, and less than 1% at 500 K, see Fig. 7(a)).

O_w–O_t bonds, on the other hand, are formed frequently, with more than one bond per molecule on average. With temperature increasing, one would expect the Gaussian–type distribution of H-bonds, such as those shown in Fig. 7(b), to widen. This is indeed the case for $T = 300$ K and $T = 400$ K. The $T = 500$ K curve is significantly shifted to the left due to the loss of some water molecules. In addition, the distribution appears less spread than the one at $T = 400$ K, for which we do not have any clear explanation at the moment.

IX. DISCUSSION AND CONCLUSIONS

We have described a lengthy and complicated fitting procedure leading to a multi-parameter tight binding model. Nevertheless, it is remarkable that the resulting model is able to faithfully reproduce a number of non trivial properties of TiO_2 that are normally controversial and uncertain even at the level of DFT and quantum chemistry calculations. In addition by combining and merging this model with our parallel work on water, we are able to make predictions about the reactive behavior of water at TiO_2 surfaces, in simulations that are beyond the capability of other methods due to the large length and time scales involved. It is due to this success as well as that reported in Papers I and II[1,2] that we can claim to have created a "universal" TB scheme that amounts essentially to a computational tool that is freely available to the community.[27] In fact it is worth recalling some of the phenomena that we are able to describe with a single parameterization of the oxygen atom: these include, the O–O radial distribution function in water and an explanation of the "fifth neighbour";[2] proton transfer and enolization in aqueous solvent;[1] transferable and quantitatively accurate description of single and double carbon–oxygen bonds;[1] the dissociation of water on TiO_2 surfaces—both stoichiometric and reduced.

We must emphasize that our approach is radically different compared to recent TB models.[76–79] Those authors take the view that an optimal TB parameter set may be discovered by explicit DFT calculations or the fitting of bond integrals and on-site energies to directly calculated integrals over projections from Kohn–Sham orbitals. This is of course an attractive approach, but in our view this leaves little room to move in the parameter space once the more fundamental parameters are firmly established. In particular the volume or bond length dependence of the on-site energies is implicit in any DFT calculation but is absent in almost all TB models. In addition the pair potentials are much more difficult to extract from a DFT calculation, except by simple subtraction of the total and band energies. As we have shown in this series of papers, careful negotiation is needed between parameter sets in order to obtain a universal model. Furthermore the nature of the hydrogen bond, which is particularly elusive, needs to be granted particular attention and is at any event beyond the reach of *ab initio* DFT.

In conclusion, we have demonstrated a TB model for TiO_2 and presented detailed results of simulations of both the infinite solid, semi infinite solid, and nanocrystalline free standing clusters. In each case we have made comparisons with established and speculative results of experiments and more accurate calculations. We have discussed the question of water adsorption at both stoichiometric and reduced surfaces and described conditions under which it would be expected that the water will dissociate. Finally, we use the model to explore the adsorption of water on anatase nanoparticles at different temperatures and demonstrate the interplay between adsorption at facets, facet edges, and corners, as well as between the potential energy and configurational entropy.

This work will be followed by large scale simulations probably leading to new predictions of the behavior of water at TiO_2. In the near future we expect to be able to model an entire process in catalysis at nanoparticle surfaces.

[1]T. J. Sheppard, A. Y. Lozovoi, D. L. Pashov, J. J. Kohanoff, and A. T. Paxton, J. Chem. Phys. **141**, 044503 (2014).

[2]A. Y. Lozovoi, T. J. Sheppard, D. L. Pashov, J. J. Kohanoff, and A. T. Paxton, J. Chem. Phys. **141**, 044504 (2014).

[3]U. Diebold, Surf. Sci. Rep. **48**, 53 (2003).

[4]C. Sun, L.-M. Liu, A. Selloni, G. Q. Lu, and S. C. Smith, J. Mater. Chem. **20**, 10319 (2010).

[5]C. L. Pang, R. Lindsay, and G. Thornton, Chem. Soc. Rev. **37**, 2328 (2008).

[6]C. L. Pang, R. Lindsay, and G. Thornton, Chem. Rev. **113**, 3887 (2013).

[7]L. Goodwin, A. J. Skinner, and D. G. Pettifor, Europhys. Lett. **9**, 701 (1989).

[8]M. W. Finnis, A. T. Paxton, M. Methfessel, and M. van Schilfgaarde, Phys. Rev. Lett. **81**, 5149 (1998).

[9]S. Fabris, A. T. Paxton, and M. W. Finnis, Phys. Rev. B **63**, 941011 (2001).

[10]M. W. Finnis, *Interatomic Forces in Condensed Matter* (Oxford University Press, Oxford, UK, 2003).

[11]A. T. Paxton, in *Multiscale Simulation Methods in Molecular Sciences*, NIC Series Vol. 42, edited by J. Grotendorst, N. Attig, S. Blügel, and D. Marx (Institute for Advanced Simulation, Forschungszentrum Julich, 2009), pp. 145–174. Also available on-line at http://webarchiv.fz-juelich.de/nic-series/volume42/volume42.html.

[12]P. A. Cox, *Transition Metal Oxides: An Introduction to Their Electronic Structure and Properties* (Oxford University Press, Oxford, UK, 2010).

[13]W. A. Harrison, *Electronic Structure and the Properties of Solids, the Physics of the Chemical Bond* (W. H. Freeman and Company, San Francisco, 1980).

[14]A. T. Paxton and J. J. Kohanoff, J. Chem. Phys. **134**, 044130 (2011).

[15]S. Fabris, A. T. Paxton, and M. W. Finnis, Phys. Rev. B **61**, 6617 (2000).

[16]N. Benedek, K. Johnston, and A. T. Paxton, unpublished results.

[17]S. Fabris, A. T. Paxton, and M. W. Finnis, Acta Mater. **50**, 5171 (2002).

[18]H.-P. Schwefel, *Numerische Optimierung von Computer–Modellen mittels der Evolutionsstrategie*, Interdisciplinary Systems Research Vol. 26 (Birkhäuser, Basle, 1977).

[19]H.-P. Schwefel, *Evolution and Optimum Seeking (Sixth Generation Computer Technologies)* (Wiley, New York, 1995).

[20]J. K. Burdett, T. Hughbanks, G. J. Miller, J. W. Richardson, and J. V. Smith, J. Am. Chem. Soc. **109**, 3639 (1987).

[21]J. K. Dewhurst and J. E. Lowther, Phys. Rev. B **54**, R3673 (1996).

[22]L.-C. Ming and M. H. Manghnani, J. Geophys. Res.: Solid Earth **84**, 4777, doi:10.1029/JB084iB09p04777 (1979).

[23]T. Arlt, M. Bermejo, M. A. Blanco, L. Gerward, J. Z. Jiang, J. S. Olsen, and J. M. Recio, Phys. Rev. B **61**, 14414 (2000).

[24]J. Pascual, J. Camassel, and H. Mathieu, Phys. Rev. Lett. **39**, 1490 (1977).

[25]H. Tang, H. Berger, P. Schmid, F. Lévy, and G. Burri, Solid State Commun. **87**, 847 (1993).

[26]S. J. Smith, R. Stevens, S. Liu, G. Li, A. Navrotsky, J. Boerio-Goates, and B. F. Woodfield, Am. Miner. **94**, 236 (2009).

[27]Empirical tight binding (TBE) and full potential LMTO computer programs (LMF) are parts of the LM electronic structure package (http://www.lmsuite.org).

[28]H. J. Monkhorst and J. D. Pack, Phys. Rev. B **13**, 5188 (1976).

[29]G. J. Martyna, M. E. Tuckerman, D. J. Tobias, and M. L. Klein, Mol. Phys. **87**, 1117 (1996).

[30]J. Muscat, V. Swamy, and N. M. Harrison, Phys. Rev. B **65**, 224112 (2002).

[31]F. Labat, P. Baranek, C. Domain, C. Minot, and C. Adamo, J. Chem. Phys. **126**, 154703 (2007).

[32]L. Chiodo, J. M. Garcia-Lastra, A. Iacomino, S. Ossicini, J. Zhao, H. Petek, and A. Rubio, Phys. Rev. B **82**, 045207 (2010).

[33]M. Landmann, E. Rauls, and W. G. Schmidt, J. Phys.: Condens. Matter **24**, 195503 (2012).

[34]G. Dolgonos, B. Aradi, N. H. Moreira, and T. Frauenheim, J. Chem. Theory Comput. **6**, 266 (2010).

[35]F. Labat, P. Baranek, and C. Adamo, J. Chem. Theory Comput. **4**, 341 (2008).

[36]M. Lazzeri, A. Vittadini, and A. Selloni, Phys. Rev. B **63**, 155409 (2001).

[37]M. Lazzeri, A. Vittadini, and A. Selloni, Phys. Rev. B **65**, 119901 (2002) [Erratum].

[38]A. Kiejna, T. Pabisiak, and S. W. Gao, J. Phys.: Condens. Matter **18**, 4207 (2006).

[39]P. M. Kowalski, B. Meyer, and D. Marx, Phys. Rev. B **79**, 115410 (2009).

[40]L. Mino, G. Spoto, S. Bordiga, and A. Zecchina, J. Phys. Chem. C **117**, 11186 (2013).

[41]T. R. Esch, I. Gadaczek, and T. Bredow, Appl. Surf. Sci. **288**, 275 (2014).

[42]X.-Q. Gong and A. Selloni, J. Phys. Chem. B **109**, 19560 (2005).

[43]A. Marmier, A. Lozovoi, and M. W. Finnis, J. Eur. Ceram. Soc. **23**, 2729 (2003).

[44]R. Lindsay, A. Wander, A. Ernst, B. Montanari, G. Thornton, and N. M. Harrison, Phys. Rev. Lett. **94**, 246102 (2005).

[45]A. Y. Lozovoi, A. Alavi, and M. W. Finnis, Phys. Rev. Lett. **85**, 610 (2000).

[46]H. Cheng and A. Selloni, J. Chem. Phys. **131**, 054703 (2009).

[47]T. Pabisiak and A. Kiejna, Solid State Commun. **144**, 324 (2007).

[48]P. Scheiber, M. Fidler, O. Dulub, M. Schmid, U. Diebold, W. Hou, U. Aschauer, and A. Selloni, Phys. Rev. Lett. **109**, 136103 (2012).

[49]A. Vittadini, M. Casarin, and A. Selloni, Theor. Chem. Acc. **117**, 663 (2007).

[50]M. B. Hugenschmidt, L. Gamble, and C. T. Campbell, Surf. Sci. **302**, 329 (1994).

[51]M. A. Henderson, Surf. Sci. **355**, 151 (1996).

[52]D. Brinkley, M. Dietrich, T. Engel, P. Farrall, G. Gantner, A. Schafer, and A. Szuchmacher, Surf. Sci. **395**, 292 (1998).

[53]H. Kamisaka and K. Yamashita, Surf. Sci. **601**, 4824 (2007).

[54]P. J. D. Lindan and C. Zhang, Phys. Rev. B **72**, 075439 (2005).

[55]A. Tilocca, C. Di Valentin, and A. Selloni, J. Phys. Chem. B **109**, 20963 (2005).

[56]W. Zhang, J. Yang, Y. Luo, S. Monti, and V. Carravetta, J. Chem. Phys. **129**, 064703 (2008).

[57]M. F. Camellone, P. M. Kowalski, and D. Marx, Phys. Rev. B **84**, 035413 (2011).

[58]Y. He, A. Tilocca, O. Dulub, A. Selloni, and U. Diebold, Nat. Mater. **8**, 585 (2009).

[59]G. S. Herman, Z. Dohnálek, N. Ruzycki, and U. Diebold, J. Phys. Chem. B **107**, 2788 (2003).

[60]Z. Zhao, Z. Li, and Z. Zou, J. Phys. Chem. C **116**, 7430 (2012).

[61]A. T. Paxton and L. Thiên-Nga, Phys. Rev. B **57**, 1579 (1998).

[62]We do not have the H_2 molecule either since we neglect any attraction between hydrogen atoms, otherwise we could have estimated the chemical potential of O, μ_O, as the difference between H_2O and H_2. The best estimation we could make is to use *experimental* energy of O_2 dissociation (with vibrations removed), 5.230 eV [Y. Zhang and W. Yang, Phys. Rev. Lett. **80**, 890 (1998)], and promotion energy of oxygen atom from the triplet to singlet state, 2.399 eV (CCSD, our own calculation) to arrive at the absolute vacancy formation energy on rutile(110) $E^f(V_O) = 2.39$ eV.

[63]J. VandeVondele, private communication (2013).

[64]A. Fujishima and K. Honda, Nature (London) **238**, 37 (1972).

[65]L. E. Walle, A. Borg, P. Uvdal, and A. Sandell, Phys. Rev. B **80**, 235436 (2009).

[66]D. A. Duncan, F. Allegretti, and D. P. Woodruff, Phys. Rev. B **86**, 045411 (2012).

[67]L. E. Walle, D. Ragazzon, A. Borg, P. Uvdal, and A. Sandell, Surf. Sci. **621**, 77 (2014).

[68]D. R. Hummer, J. D. Kubicki, P. R. C. Kent, J. E. Post, and P. J. Heaney, J. Phys. Chem. C **113**, 4240 (2009).

[69]M. A. Henderson, Surf. Sci. Rep. **66**, 185 (2011).

[70]H. Zhang and J. F. Banfield, J. Mater. Chem. **8**, 2073 (1998).

[71]B. Montanari and N. M. Harrison, J. Phys.: Condens. Matter **16**, 273 (2004).

[72]G. Lever, D. J. Cole, N. D. M. Hine, P. D. Haynes, and M. C. Payne, J. Phys.: Condens. Matter **25**, 152101 (2013).

[73]Y. Zhou and K. A. Fichthorn, J. Phys. Chem. C **116**, 8314 (2012).

[74]A. Selloni, Nat. Mater. **7**, 613 (2008).

[75]The definition of bonds in our study is based on the position of the first minimum in radial distribution functions for respective species, which are: 3.4 Å for Ti–Ti, 2.7 Å for Ti–O_t, 2.9 Å for Ti–O_w, 3.6 Å for O_t–O_t, and

3.2 Å for both O_t–O_w and O_w–O_w. The O_t–O_w and O_w–O_w distances in particular are used in the definition of water–water and water–titania H-bonds together with the 30° criterion for the $\widehat{HOO}$ angle [A. Luzar and D. Chandler, Phys. Rev. Lett. **76**, 928 (1996)].

[76] S. Sanna, B. Hourahine, T. Gallauner, and T. Frauenheim, J. Phys. Chem. **111**, 5665 (2007).

[77] G. K. H. Madsen, E. J. McEniry, and R. Drautz, Phys. Rev. B **83**, 184119 (2011).

[78] A. Urban, M. Reese, M. Mrovec, C. Elsässer, and B. Meyer, Phys. Rev. B **84**, 155119 (2011).

[79] N. Hatcher, G. K. Madsen, and R. Drautz, Phys. Rev. B **86**, 155115 (2012).